Monte Carlo evaluation of the muon-induced background in the GERDA double beta decay experiment

L. Pandola[a], M. Bauer[b], K. Kröninger[c], X. Liu[c], C. Tomei[a], S. Belogurov[d,e],
D. Franco[f], A. Klimenko[d,g] and M. Knapp[b]

INFN - Laboratori Nazionali del Gran Sasso

Monte Carlo evaluation of the muon-induced background in the GERDA double beta decay experiment

L. Pandola[a], M. Bauer[b], K. Kröninger[c], X. Liu[c], C. Tomei[a], S. Belogurov[d,e],
D. Franco[f], A. Klimenko[d,g] and M. Knapp[b]

[a] *INFN, Laboratori Nazionali del Gran Sasso, Assergi, Italy*
[b] *Physikalisches Institut, Eberhard Karls Universität Tübingen, Germany*
[c] *Max-Planck-Institut für Physik, München, Germany*
[d] *Institute for Nuclear Research of the Russian Academy of Sciences, Moscow, Russia*
[e] *Institute for Theoretical and Experimental Physics, Moscow, Russia*
[f] *Max-Planck-Institut für Kernphysik, Heidelberg, Germany*
[g] *Joint Institute for Nuclear Research, Dubna, Russia*

Abstract

The new generation of experiments searching for neutrinoless double beta decay are aiming at a background level of 10^{-3} counts/(kg·keV·y) or better at the respective Q-values. Cosmic ray muons can be a significant contribution due to a number of physics processes. The GERmanium Detector Array, GERDA, located at the Gran Sasso underground laboratory in Italy, uses germanium enriched in ^{76}Ge as source and detector material. Germanium is submerged into liquid nitrogen or argon that acts as cooling medium and radiation shield simultaneously. A detailed GEANT4-based Monte Carlo simulation was performed to calculate the photon and neutron fluxes induced by cosmic ray muons. The prompt background contributions from γ-ray and neutron interactions as well as the delayed contributions due to the production of radioactive isotopes within the setup are given. The background can be reduced to the desired level with the muon veto system incorporated in the GERDA design.
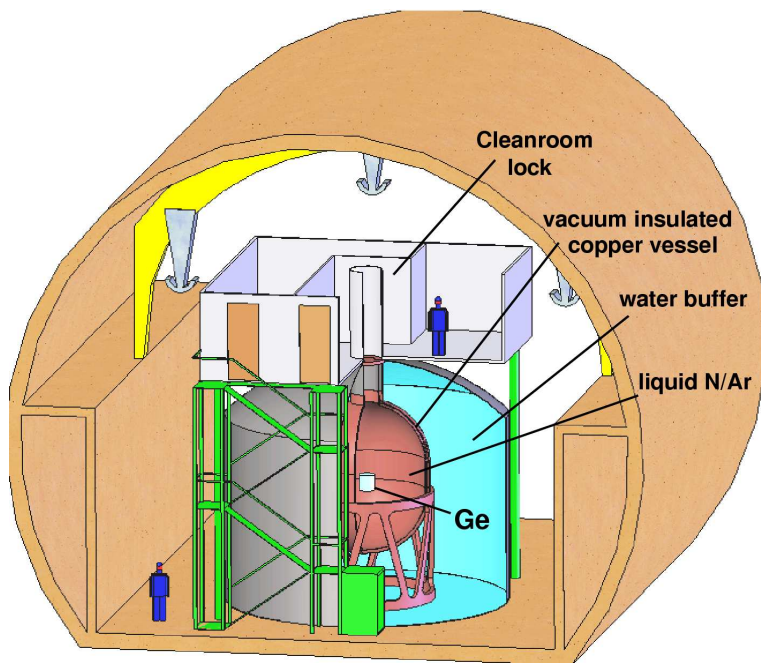
Figure 1: Schematic view of the design of the GERDA experiment.

1   Introduction

The GERmanium Detector Array, GERDA [1], is designed to search for neutrinoless double beta decay ($0\nu\beta\beta$) of ^{76}Ge. The importance of such a search is emphasized by the evidence of non-vanishing neutrino masses from flavor oscillations and by the recent claim based on data of the Heidelberg-Moscow experiment [2]. GERDA will be installed in Hall A of the INFN Gran Sasso National Laboratory (LNGS). The experiment is designed to collect about 100 kg·y of quasi background-free data. This leads to the requirement of a background index of the order of 10^{-3} counts/(kg·keV·y) around the $Q_{\beta\beta}$ value of 2039 keV [3]. The main design feature of GERDA is to use the cryogenic liquid (nitrogen or argon) as the shield against the external γ radiation [4]. External γ-rays resulting from the cryostat and the Cu/Pb shields were found to be the dominating background source in earlier experiments [2, 5]. In the GERDA design high purity germanium detectors are immersed directly in the cryogenic liquid which is also the cooling medium. The cryogenic volume is surrounded by a buffer of ultra-pure water acting as an additional γ and neutron shield (see Fig. 1).

The experiment is foreseen to proceed in two phases. In the first phase detectors, enriched in ^{76}Ge, that were previously operated by the Heidelberg-Moscow and IGEX collaborations will be redeployed. At this stage the background might be limited to 10^{-2} counts/(kg·keV·y) due to intrinsic ^{60}Co contamination of the existing detectors. In the second phase new detectors will be installed. They will be produced with special care taken to reduce the cosmogenically produced radioactive contaminants. In addi-
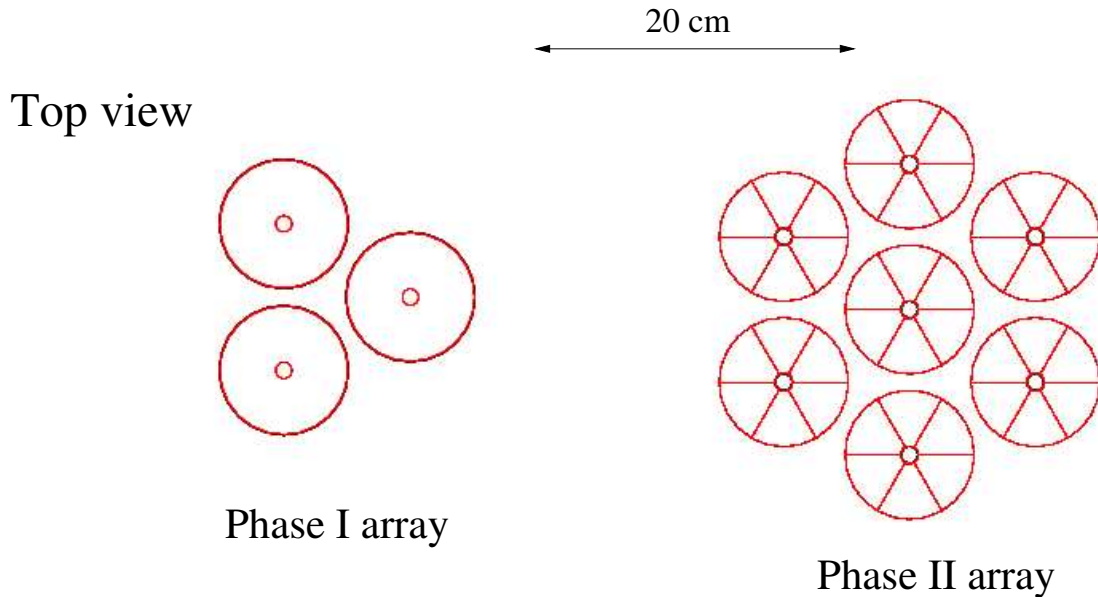
20 cm

Top view

Phase I array

Phase II array

Figure 2: Top view of the detector arrays for phase I (9 crystals) and phase II (21 crystals). The detectors are mounted in three layers. The vertical separation between the layers is 50 mm. The 6-fold azimuthal segmentation is visible for the phase II detectors.

tion, these detectors will be segmented. The currently envisioned segmentation scheme is 18-fold with 6 segments in the azimuthal angle φ and 3 axial segments. The existing detectors have a mass of approximately 2 kg each. The phase II detectors are still under design, but are expected to be of similar dimensions. For this study we use two "ideal" setups. Phase I has 9 detectors arranged in a 3 × 3 matrix. Phase II has 21 detectors arranged in a hexagonal package of 7 × 3. All detectors are assumed to have diameter and height of 80 mm and a distance of closest approach of 10 mm. A visualization of the detector arrays is given in Fig. 2.

Cosmic ray muons crossing the setup and the surrounding materials can interact and create an effective flux of secondary particles in the detector array. Most important are the γ-rays and neutrons. Their interactions can produce a prompt energy deposition faking the signature of a neutrinoless double beta decay, i.e. a localized energy deposition of approximately 2039 keV. In addition radioactive isotopes can be produced which can cause a delayed background contribution. The prompt component can be reduced effectively by an active muon veto. The reduction factor possibly achievable for the delayed component depends on the life time and the decay scheme of the produced radioactive isotope.

Since the GERDA goal for the total background index in the second phase is 10^{-3} counts/(kg·keV·y), the contribution of each of the background components (muons, external γ-rays, internal contamination, etc.) should not exceed 10^{-4} counts/(kg·keV·y). Thus, the maximum tolerable background from prompt and delayed muon interactions is 10^{-4} counts/(kg·keV·y) each.

3

It has been pointed out in Ref. [6] that a ^{76}Ge double beta decay experiment having a massive Cu/Pb shield surrounding the sensitive material could be limited by the muon-induced neutron background. The background would mainly come from inelastic interactions of these neutrons in Ge, Cu and Pb. According to Ref. [6], if an experiment like Majorana [7] were placed at the depth of the Gran Sasso laboratory, the muon-induced background would be about $4 \cdot 10^{-3}$ counts/(kg·keV·y), where a 90% efficient muon veto is assumed. The results presented here demonstrate that the situation is more favorable for the GERDA design because: (1) the detectors are surrounded by low-Z materials and (2) the water buffer acts as a shield against neutrons produced by muons in the surrounding rock. This results, together with the muon veto envisioned, in background rates as low as 10^{-4} counts/(kg·keV·y).

The paper is organized as follows: in Sect. 2 the assumptions of the Monte Carlo simulation concerning the experimental setup and the primary spectrum are described. In Sect. 3 the muon-induced fluxes of neutrons and γ-rays in the vicinity of the detectors are presented. The prompt background rate and the efficiency of the muon veto required to reduce it to below 10^{-4} counts/(kg·keV·y) are described in Sect. 4. The delayed background due to unstable isotopes induced by secondaries from muon interactions is presented in Sect. 5. In Sect. 6 the conclusions are drawn.

2 Simulation

2.1 Muon spectrum

The Gran Sasso overburden of 3400 m w.e. suppresses the cosmic muon flux by six orders of magnitude to 1.1 muons/(m^2·h) [8] and shifts the mean energy to 270 GeV [9]. The energy spectrum of cosmic ray muons in Hall A of the laboratory is calculated according to the analytical parametrization of Ref. [10], which is in agreement with the experimental data of Ref. [9]. The energy range spans from 1 GeV to 10 TeV, as shown in Fig. 3. The range includes 99.2% of the total muon flux. The angular distribution is determined by the profile of the Gran Sasso mountain and it has been precisely measured by the MACRO experiment [11]. The distribution used for the simulation is hence calculated from this measurement. The average zenith angle is $\langle \theta \rangle \sim 35$ degrees. The distribution of the azimuth angle φ is not uniform, but follows the profile of the mountain. Separate projections of the distribution in $\cos \theta$ and φ are shown in Fig. 4.

2.2 GERDA geometry

The full technical details of the complete GERDA setup are not yet available. The geometry implemented in the simulation is shown in Fig. 5. The infrastructural material on top and on one side of the setup is not included. This is a reasonable simplification, since the secondary particles produced in the materials outside the water tank (rock, infrastructures) are effectively absorbed by the water buffer (see Sect. 4.2).

The simulated setup has a cryogenic volume of about 45 m^3 filled with either liquid
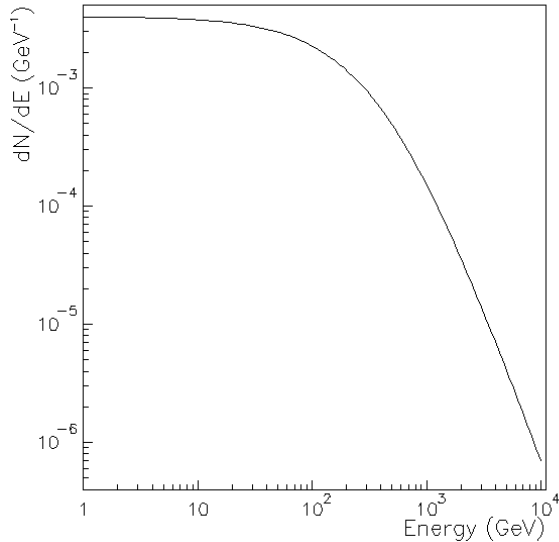
4

Figure 3: Energy spectrum of cosmic ray muons in the Gran Sasso underground laboratory according to the parametrization of Ref. [10].

nitrogen or liquid argon. The volume is surrounded by three copper walls. The thickness of each of the copper walls is assumed to be 2 cm. The cryostat is modeled with a central cylindrical part ($r = 2$ m, $h = 1$ m) and two hemispheres ($r = 2$ m), as depicted in Fig. 5. The neck is defined as a single steel wall. The water volume is contained by a cylindrical stainless-steel tank of radius 5 m and height 8.9 m. The thickness of the steel walls is 10 mm. The total amount of water foreseen in this design is about 700 t. The ideal detector arrays for phase I or II as defined above are located in the center of the cryogenic volume. An energy threshold of 50 keV is assumed for a germanium detector or a detector segment, respectively. This is a conservative assumption: the threshold foreseen for the detector array is 10 keV and the efficiency of the background rejection based on crystal/segment anticoincidence is improved with a lower threshold. The dead layers of the detectors are taken into account in the simulation.

Two muon vetoes are incorporated in the GERDA design. Primarily, the water buffer is operated as a Čerenkov detector, with a design similar to the Borexino experiment [12]. Photomultipliers (PMTs) immersed in the water detect the visible Čerenkov light. The walls are covered by a reflector foil in order to increase the light collection. In addition a plane of plastic scintillator (5×5 m^2) of 5 cm thickness is placed on the top of the setup to detect vertical muons which may channel through the neck and fail to give a signal in the Čerenkov detector. The thresholds assumed are 120 MeV for the water veto (this corresponds to 60 cm track length and about 18,000 Čerenkov optical photons) and 4 MeV for the plastic scintillator. The threshold of the water Čerenkov detector has been set to ensure a high detection efficiency for those muon-induced events that produce an energy
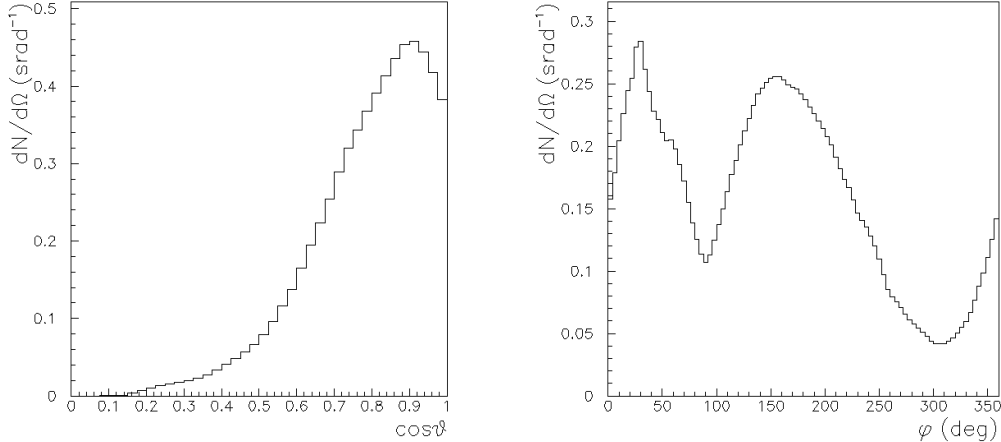
Figure 4: Separate projections of the muon angular distribution in $\cos\theta$ and φ from the MACRO measurements [11].

deposit in the germanium crystals[1]. The threshold of the plastic scintillator gives a high detection efficiency for crossing muons but is above the energy of the environmental γ-rays (2.6 MeV from ^{208}Tl) which would otherwise dominate the trigger rate (0.5 kHz/m^2).

2.3 Geant4 and systematic uncertainties

The Monte Carlo simulation of the muon-induced background has been carried out using the GEANT4-based [13] MAGE framework [14] which is jointly developed and maintained by the GERDA and Majorana Monte Carlo groups. The MAGE physics list has been chosen to handle both low energy interactions and hadronic interactions resulting from cosmic ray spallation[2]. The suitability of the GEANT4 toolkit in the context of underground physics has been demonstrated in a number of Monte Carlo studies, including the simulation of the Heidelberg-Moscow detector, that can be found in the present literature, both for double beta decay and for dark matter experiments [16, 17]. The GEANT4 bug reported in Ref. [18], which affects the neutron inelastic interactions in germanium, has been fixed. The electromagnetic component dominates the prompt muon-induced background in GERDA. The relevant GEANT4 physics processes have been extensively and systematically validated by the GEANT4 Collaboration [19] and by other groups [20] at

---

[1]Muons having a path in water of less than 60 cm cannot be detected. Such muons do not produce secondaries that reach the cryogenic liquid or the vicinity of the detectors and are thus not relevant.

[2]The MAGE physics list is mainly based on "underground physics" advanced example (LBE) which is distributed with the GEANT4 package [15]. Theory-driven quark-gluon string models (QGSP) are used for the reactions of energetic pions, kaons, and nucleons. Inelastic interactions of pions and nucleons below 10 GeV are described by the Binary cascade model (BIC). In addition tabulated cross-section data are used to model capture, elastic scattering and inelastic scattering of neutrons from thermal energies up to 20 MeV (HP models).
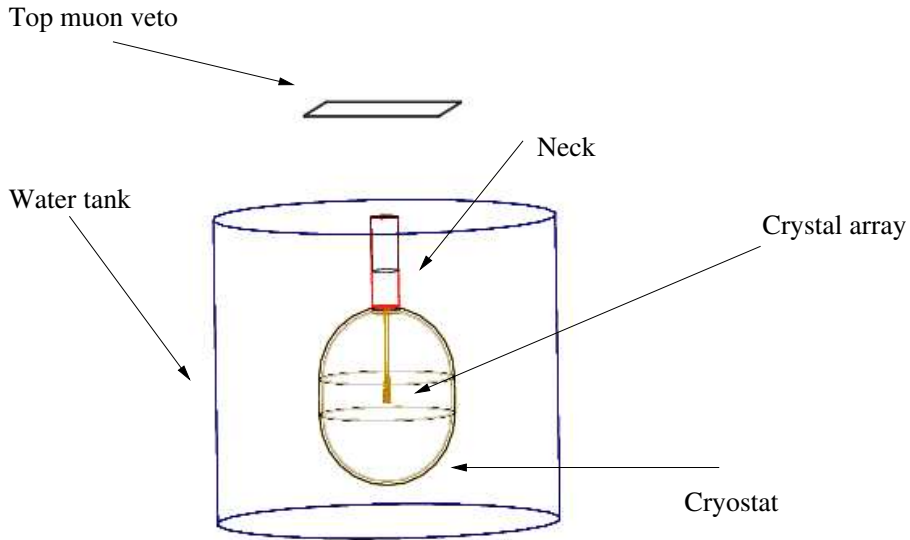
Figure 5: Geometry implemented in the simulation of the GERDA setup.

the few-percent level. The systematic uncertainty of the γ-ray flux and consequently the prompt background is mainly due to the uncertainty of flux and spectrum of the primary muons. It is estimated to be 10%, according to Ref. [21].

The systematic uncertainty of the neutron flux and the isotope production is more difficult to estimate. The predictions of GEANT4 for the muon-induced neutron yield in organic scintillators [22] are found to be in agreement with the data from the LVD experiment [23] in the Gran Sasso laboratory. As pointed out in Ref. [22], experimental data for neutron production by energetic muons in heavy target are scarce and mutually inconsistent. The muon-induced neutron yield in materials with $Z < 40$ determined by GEANT4 agrees with the prediction of the FLUKA code [24] within 40%, while the integral neutron fluxes differ by about 20-30% because of the different treatment of the elastic scattering in the two codes [22]. The systematic uncertainty for the neutron flux and the isotope production is assumed to be 40%.

An equivalent statistics of about 6 years ($\approx 70 \cdot 10^6$ primary muons) is generated for each phase and for the two options of the cryogenic liquid. The CPU time required on a 2.4 GHz clock 64-bit PC is about 22 minutes for the statistics equivalent to one day.

3 Neutron and Gamma Ray Fluxes

The γ-ray and neutron fluxes induced by muons in the detector region are calculated dividing the total number of particles entering a sphere ($r = 30$ cm) containing the detector array by the cross section of the sphere. The effective γ-ray and neutron fluxes

7

Table 1: Effective γ-ray and neutron fluxes in the detector region for the standard configuration of the simulation geometry and a special one without water buffer and tank. The fraction of the neutron flux below 1 keV is about 10%. Only statistical errors are quoted. Systematic uncertainties are discussed in the text.

Geometry	γ-ray $> Q_{\beta\beta}$ particles/(m$^2\cdot$ h)	Neutrons (integral) particles/(m$^2\cdot$ h)
Nitrogen		
Crystals, cryogenic liquid and cryostat only	0.272 ± 0.005	0.056 ± 0.003
Full detector	5.4 ± 0.2	0.72 ± 0.03
Argon		
Crystals, cryogenic liquid and cryostat only	6.28 ± 0.03	2.37 ± 0.02
Full detector	9.76 ± 0.05	5.72 ± 0.04

are shown in Tab. 1.

In order to understand the development of the neutron and γ-ray fluxes in muon-induced cascades, the Monte Carlo simulation was run with different geometries. Beside the standard a special geometry omitting the water buffer and tank was studied. In the special geometry only the cryostat, the cryogenic liquid and the crystals themselves are available for the development of cascades. The results are summarized in Tab. 1.

The γ-ray and neutron fluxes are significantly lower in liquid nitrogen than in liquid argon in both geometries. For the γ-ray flux this is due to: (1) the critical energy at which the radiative energy losses of electrons are equal to ionization losses being larger (about 100 MeV), as it scales as $1/Z$ [25]; (2) the thickness of the cryogenic layer being only about four times the radiation length in liquid nitrogen which is $x_0 = 47$ cm. Therefore, the electromagnetic showers do not fully develop in liquid nitrogen. Similarly, the layer thickness is also insufficient for the full development of muon-induced hadronic cascades. Most of the γ-ray and neutron fluxes in the liquid nitrogen setup is therefore produced in the water buffer.

In the liquid argon setup the contribution to the neutron flux produced by nuclear cascades in the cryogenic liquid itself is sizable due to the higher density and higher Z of argon. The radiation length in liquid argon is only $x_0 = 14$ cm. In this case the cryogenic layer is about 14 radiation lengths thick which is enough to allow the full development of electromagnetic showers as well as absorption of γ-rays produced in the water. The γ-ray flux therefore only increases by a factor of about 1.5 when adding the water buffer.

The neutron flux in the complete setup with argon is a factor of eight higher than in nitrogen. This is the combined result of two effects:

1. the neutron yield in liquid argon is about four times larger than in liquid nitrogen. According to Monte Carlo simulations, the neutron yield from muon interactions is roughly proportional to $A^{0.8} \cdot \rho$, where A is the atomic mass and ρ is the density [6, 22, 26].

2. argon is less efficient than nitrogen as a neutron moderator, because of the smaller average energy transfer per elastic interaction.

In summary there is a significant γ-ray and neutron production by cosmic muons in the water buffer. This has different influences on the particle flux in the central volume depending on the cryogenic liquid chosen: in the case of liquid nitrogen the photons are shielded less efficiently whereas the neutrons are well moderated. For argon the γ-rays are well shielded, whereas more neutrons are propagated.

Neglecting the possibility of specific effects of nuclear physics, it can be assumed that the results reported in Tab. 1 are still qualitatively valid, if the copper is replaced by a comparable amount of stainless steel as discussed in the GERDA backup design [1]. This is due to the similarity of the density and the average atomic mass $\langle A \rangle$ of the two materials.

4   Prompt Background

Both γ-rays and neutrons contribute to the prompt background. γ-rays deposit energy in the crystals through electromagnetic interactions. The neutron-induced prompt background is due to the photons emitted in (n,n'γ) or (n,γ) interactions. Nuclear recoils from neutron elastic scattering do not contribute at $Q_{\beta\beta}$ for two reasons: (1) the ionization yield for nuclear recoils in germanium is a factor of three smaller than for electrons [27]. Therefore a 2-MeV electron-equivalent energy deposition corresponds to a 6-MeV nuclear recoil; (2) the mass of germanium nuclei is large with respect to the neutron mass. Therefore only a small fraction of energy can be transfered in elastic interactions.

4.1   Muons crossing the setup

The rate in the liquid nitrogen setup of muon-induced events in which at least one detector is triggered is 120 events/(kg·y) (= 6 events/day) in phase I and 75 events/(kg·y) (= 9 events/day) in phase II. The average number of crystals with an energy deposition above threshold in these events is 2.6 (3.9) in phase I (phase II); the average number of segments with an energy deposition above threshold in phase II is 11 per event. The integral rates in the argon scenario are 10% smaller, although the component below 3 MeV is 30-40% larger than for nitrogen.

   The energy deposition in the germanium detectors is dominated by muons themselves and the induced γ-ray flux. The spectra in the crystals are displayed in Fig. 6 for liquid nitrogen. They are approximately flat above 1 MeV. The background index at $Q_{\beta\beta}$ is evaluated within an energy window from 1.5 MeV to 2.5 MeV. The resulting values without any anticoincidence cuts are 1.43±0.04(stat)±0.14(syst) ·10^{-2} counts/(kg·keV·y) for liquid nitrogen and 1.90±0.04(stat)±0.19(syst) ·10^{-2} counts/(kg·keV·y) for liquid argon. Since most $0\nu\beta\beta$-decay events are single-site events, i.e. the energy is deposited locally
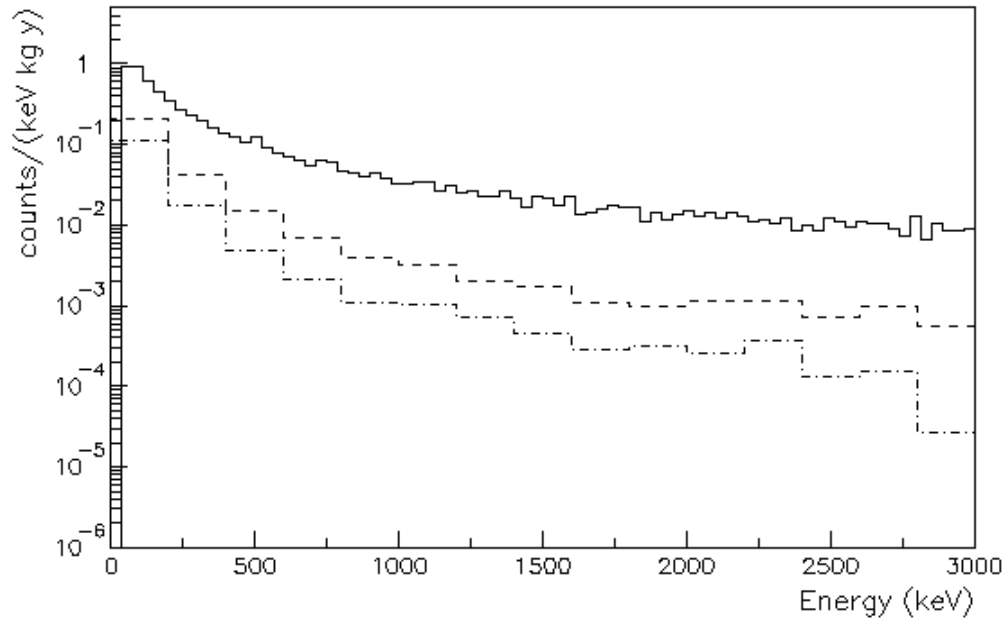
Figure 6: Energy spectrum as seen by individual crystals in liquid nitrogen without any cut (solid line) in the energy range between 50 keV and 3 MeV. The dashed/dot-dashed spectrum describes events with only one crystal/segment hit. Such events are selected by a crystal anticoincidence cut (phase I) or a segment anticoincidence cut (phase II), respectively. The mass of each crystal is 2 kg.

by the final-state electrons, background from γ-rays and muons can effectively be suppressed by requiring that only one crystal or segment shows an energy deposition, leading to anticoincidence requirements between crystals or segments [28]. In principle the discrimination between single-site and multi-site events can be further improved by using algorithms of pulse shape analysis [29, 30]. In the present work the background reduction achievable by pulse shape discrimination is not accounted for. The dashed (dot-dashed) histogram in Fig. 6 shows the same spectrum after the anticoincidence cut between the detectors (the segments) has been applied. The crystal anticoincidence cuts reduce the background by a factor of about 14 and 25 in phase I and II in the interesting energy region, respectively[3]. An other factor of two is gained in phase II with the segment anticoincidence cuts. The resulting background indices are summarized in Tab. 2. The background is 30-40% larger in the argon option. Qualitatively this is expected from the neutron and γ-ray fluxes quoted in Tab. 1 and from the different mean free path of γ-rays in argon and nitrogen.

The goal background of 10^{-4} counts/(kg·keV·y) for the prompt muon component can be achieved with a dedicated and efficient muon veto system, as discussed in Sect. 4.3.

4.2 Muons not crossing the setup

In Sect. 4.1 only muons interacting in the setup are accounted for. There is the additional possibility that muons interacting in the surrounding rock create high-energy neutrons that are entering the experimental setup. They can penetrate the shield and contribute to the background around $Q_{\beta\beta}$. Since the explicit Monte Carlo tracking of muons and neutrons in thick layers of rock is extremely CPU-intensive, a simplified approach is chosen. High-energy neutrons from the rock are generated according to the energy and angular distributions obtained in the simulation of Ref. [26] and are tracked into the GERDA setup. The integral flux above 1 MeV is assumed to be 300 neutrons/(m^2·y), according to Ref. [26]. The mean energy is about 100 MeV.

The resulting background index for phase II is $6 \cdot 10^{-5}$ counts/(kg·keV·y). It can be reduced below 10^{-5} counts/(kg·keV·y) (90% CL) with the segment anticoincidence cut. High-energy external neutrons represent a limiting background in the calculations of Ref. [6]. However, they are effectively absorbed by the thick layer of water in the GERDA design. The contribution from muons passing in the rock is small compared to those crossing the detector. The value given should be regarded as a conservative estimate: the primary muon, which is not accounted for in this approach, could in fact cross the setup as well and trigger the veto. The fraction of neutrons reaching a distance from the primary muon track larger than the radius of the water buffer (i.e. 5 m) is about 10^{-3} [6].

---

[3]If the energy threshold of the germanium crystals or segments is set to 10 keV, the efficiency of the anticoincidence cuts is improved by 5%, while the total counting rate of the detectors is increased by 10%.

4.3 Efficiency of muon veto system

The final background index related to prompt interactions induced by muons crossing the setup depends on the overall veto efficiency. The simulation shows that all events depositing energy in the germanium detectors release at least 120 MeV in the water buffer. This yields an upper limit of about 10^{-5} counts/(kg·keV·y) for an ideal 100%-efficient veto system. The background from prompt muon interactions can be reduced in both phases below 10^{-4} counts/(kg·keV·y), provided the efficiency of the Čerenkov veto above 120 MeV is not smaller than the values reported in Tab. 3. In phase II it is about 70% for the nitrogen setup and 80% for the argon setup. The efficiency of the Čerenkov system depends on the number of PMTs and their placement.

One can compare the efficiency required for GERDA with the Čerenkov muon veto (Outer Veto) foreseen in the Borexino experiment [12]. The Borexino Outer Veto is viewed by 208 encapsulated 8-inch PMTs, giving a photocathode coverage of about 1%. The quantum efficiency averaged over the Čerenkov wavelength spectrum is about 15% [31]. The walls of the Borexino tank are covered by Tyvek reflection foils increasing the light collection efficiency by a factor of six [31]. The photoelectron yield achieved for muon tracks is about 2-3 p.e./cm. The GERDA Čerenkov veto is conceptually similar to the Borexino one, as 8-inch PMTs and light-reflecting foils are used. If the Borexino photoelectron yield is assumed, a sufficient number of photoelectrons to efficiently trigger above 120 MeV (60-cm long tracks) should be achieved in GERDA with a smaller photocathode coverage (0.5%), corresponding to $80-100$ 8-inch PMTs. The optimization of the PMT placement in the water tank is currently in progress by means of dedicated Monte Carlo simulations. Preliminary results show that a veto efficiency above 90% can be achieved for the muon tracks yielding an energy deposition in the germanium crystals using about 80 PMTs when making the assumptions stated above.

The trigger rate of the vetoes is about 2.5 events/minute for the water detector and 0.5 events/minute for the plastic scintillator.

5 Delayed background

The production of unstable isotopes inside the setup can be induced either by neutrons, via capture or other inelastic interactions as (n,p) and (n,α), or by γ-rays via photo-nuclear reactions.

The delayed decay of these nuclei can mimic $0\nu\beta\beta$-events and thus they represent an additional background source. They cannot be identified by the muon veto and form an irreducible background contribution which eventually limits the achievable background index for the given setup. The isotopes that are potential background sources for GERDA are those emitting γ and/or β rays above $Q_{\beta\beta}$ with a half-life of more than a few seconds. The β-rays are only relevant if the unstable isotope is located inside the detector crystals themselves. External β-rays are absorbed by a few millimeters of the cryogenic liquid. The isotopes produced inside the crystals are indeed the most pernicious, because also γ-rays produced there are detected with high efficiency.

Table 2: Background index in the range from 1.5 to 2.5 MeV, for different veto scenarios. Only statistical errors are quoted. A discussion of the systematic uncertainties can be found in the text.

Condition	Background index counts/(kg·keV·y)	
	Phase I	Phase II
Nitrogen		
No cuts	$(1.43 \pm 0.04) \cdot 10^{-2}$	
Crystal anticoincidence	$(1.0 \pm 0.1) \cdot 10^{-3}$	$(5.6 \pm 0.6) \cdot 10^{-4}$
Segment anticoincidence	$-$	$(2.9 \pm 0.4) \cdot 10^{-4}$
Anticoincidence + ideal muon veto	$< 3 \cdot 10^{-5}$ (95% CL)	$< 1 \cdot 10^{-5}$ (95% CL)
Argon		
No cuts	$(1.90 \pm 0.04) \cdot 10^{-2}$	
Crystal anticoincidence	$(1.6 \pm 0.1) \cdot 10^{-3}$	$(9.0 \pm 0.6) \cdot 10^{-4}$
Segment anticoincidence	$-$	$(4.0 \pm 0.4) \cdot 10^{-4}$
Anticoincidence + ideal muon veto	$< 3 \cdot 10^{-5}$ (95% CL)	$< 1 \cdot 10^{-5}$ (95% CL)

Table 3: Efficiency required for the muon veto above 120 MeV to reduce the prompt muon-induced background below 10^{-4} or 10^{-5} counts/(kg·keV·y). The effect of the crystal (segment) anticoincidence cut is taken into account for phase I (phase II).

Condition	Veto efficiency for background index	
	10^{-4} counts/(kg·keV·y)	10^{-5} counts/(kg·keV·y)
Nitrogen - phase I	90%	-
Nitrogen - phase II	65%	97%
Argon - phase I	94%	-
Argon - phase II	75%	97%

Table 4: Most relevant unstable isotopes with Q-value larger than $Q_{\beta\beta}$ that can be produced in the enriched germanium detectors and in liquid argon by muon-induced interactions [32].

Isotope	$T_{1/2}$	Q-value (keV)
^{74}Ga	8.1 m	5368
^{75}Ga	126 s	3392
^{76}Ga	33 s	7010
^{68}Ge/^{68}Ga	271 d / 68 m	106 / 2921
^{69}Ge	39 h	2227
^{77}Ge	11.3 h	2702
^{77m}Ge	53 s	2861
^{38}Cl	37 m	4916
^{40}Cl	1.4 m	7482

The production rate of unstable isotopes is evaluated from the Monte Carlo simulation. The most relevant isotopes with Q-value above $Q_{\beta\beta}$ produced in the crystals are summarized in Tab. 4. The total production rate in the crystal depends on the cryogenic liquid because of the different flux of neutrons and γ-rays. Results are presented in Tab. 5. The largest contribution comes from ^{77}Ge and ^{77m}Ge that are produced by thermal neutron capture of ^{76}Ge [33]. The isomeric state ^{77m}Ge is particularly dangerous because it is dominantly a pure β-emitter, without emission of further γ-rays [32]. The efficiency of the anticoincidence cut is therefore reduced: only 15% of the events with energy deposit around $Q_{\beta\beta}$ can be rejected using the segmentation[4].

The background due to unstable isotopes produced in the water and the cryostat walls is smaller than 10^{-6} counts/(kg·keV·y), because the probability that the radiation reaches the detector array is extremely small. The contribution from isotopes in the liquid nitrogen is smaller than 10^{-6} counts/(kg·keV·y) while it amounts to about $4 \cdot 10^{-5}$ counts/(kg·keV·y) in liquid argon. The latter can be reduced to $1.5 \cdot 10^{-5}$ using the segment anticoincidence cut.

The production of radioactive isotopes induced by muons in the GERDA setup gives a contribution to the background index around $Q_{\beta\beta}$ of the order of 10^{-4} counts/(kg·keV·y) in the liquid argon option and of 10^{-5} counts/(kg·keV·y) in the liquid nitrogen one. The ^{77m}Ge background is the dominant contribution. It can be rejected by means of delayed triple coincidence between the muon veto, the prompt γ-rays emitted in the capture and the following β decay. Although the prompt γ-ray cascade is poorly known, the total energy amounts to 6.07 MeV [34]. In the most pessimistic case (namely, all the energy is emitted in a single photon) the efficiency of the rejection cut is larger than 50%.

---

[4]This is comparable to the fraction of genuine $0\nu\beta\beta$-events that would be rejected by the segmentation cut, 14%.

Table 5: Muon-induced isotope production. The background index is calculated for phase II. It does *not* take into account the additional rejection from the segment antico-incidence and from other tools (e.g. delayed coincidences). Isotopes giving a background index below 10^{-6} counts/(kg·keV·y) are not reported. Only statistical errors are quoted. Upper limits are quoted at 90% CL. Systematic uncertainties are discussed in the text.

	Nitrogen		Argon	
	nuclei/(kg·y)	cts/(kg·keV·y)	nuclei/(kg·y)	cts/(kg·keV·y)
Isotopes produced in crystals				
^{74}Ga/^{75}Ga/^{76}Ga	< 0.08	$< 3 \cdot 10^{-5}$	< 0.1	$< 4 \cdot 10^{-5}$
^{68}Ge	0.07±0.03	$(4 \pm 2) \cdot 10^{-6}$	0.08±0.03	$(5 \pm 2) \cdot 10^{-6}$
^{69}Ge	0.38±0.08	$(1.0 \pm 0.2) \cdot 10^{-6}$	1.8±0.2	$(5.0 \pm 0.6) \cdot 10^{-6}$
^{77}Ge/^{77m}Ge	0.05±0.03	$(1.0 \pm 0.6) \cdot 10^{-5}$	0.51±0.09	$(1.1 \pm 0.2) \cdot 10^{-4}$
Isotopes produced in cryogenic liquid				
^{38}Cl	-	-	46±1 ev/day	$(3.3 \pm 0.1) \cdot 10^{-5}$
^{40}Cl	-	-	2.7±0.1 ev/day	$(4.0 \pm 0.2) \cdot 10^{-6}$

6   Conclusions

Muon-induced interactions in the GERDA experiment were extensively simulated with the GEANT4-based MAGE package in order to quantify the induced background in the $Q_{\beta\beta}$ region and to establish the required efficiency of the muon-veto system. Two options, namely nitrogen and argon, were considered for the cryogenic liquid in the central volume around the germanium detectors. The muon-induced fluxes of neutrons and γ-rays in the vicinity of the detectors are larger in the argon case than for nitrogen. This is related to the larger density, atomic number and atomic mass affecting the development of electro-magnetic and hadronic showers and neutron moderation.

The energy region between 1.5 and 2.5 MeV, where the spectrum is approximately flat, was used to evaluate the background index at $Q_{\beta\beta} = 2039$ keV from prompt processes. The rate for nitrogen in the case of no cuts is $1.4 \cdot 10^{-2}$ counts/(kg·keV·y). If a straight-forward anticoincidence between the crystals or the segments is applied, it can be reduced to 10^{-3} and $3 \cdot 10^{-4}$ counts/(kg·keV·y) in phase I and phase II, respectively. The prompt background at $Q_{\beta\beta}$ is about 30% larger for the argon setup.

To meet the GERDA specifications the muon-induced background index has to be lowered to 10^{-4} counts/(kg·keV·y). This is done by a dedicated muon veto system. The efficiency of the water veto above 120 MeV must be larger than about 80% for phase II. This can be achieved using a standard design and a relatively modest photocathode coverage of about 0.5%.

The background from the decay of long-lived unstable isotopes produced by muon in-duced interactions is potentially dangerous, because it cannot be eliminated by the veto

system. The dominant source is ^{77m}Ge produced by thermal neutron capture in ^{76}Ge. It can be reduced below the level of 10^{-4} counts/(kg·keV·y) in the liquid argon scenario making use of dedicated cuts based on delayed coincidences. The background index is one order of magnitude smaller in liquid nitrogen scenario, because of the smaller flux of muon-induced neutrons.

The GERDA goal of a background index of 10^{-4} counts/(kg·keV·y) for the muon-induced contribution can be achieved for both liquid nitrogen and argon, if the muon veto and the additional background rejection tools are used. Thus, the muon-induced background does not limit the expected GERDA sensitivity. Especially, GERDA is not limited by neutrons produced by muons interactions in the rock. The background contribution from this source is about 10^{-5} counts/(kg·keV·y).

The muon-induced background, in particular the part related to the neutron flux, is strongly dependent on the experimental design. Material properties and placement around the detectors are important. Experiments with compact high-Z passive shieldings placed close to the detectors require deeper locations to reduce the neutron and γ-ray flux induced by muon interactions in the setup itself or in the surrounding rock. The shielding design has to be optimized in a compromise between the suppression of the external radiation and the reduction of muon-induced secondary particles in the setup. The GERDA compromise is a thick passive shield of low-Z material. This design fulfills the background specifications with respect to muon-induced radiation at the depth of the Gran Sasso laboratory.

7   Acknowledgments

References

[1] GERDA Collaboration, I. Abt *et al.*, GERDA: The GERmanium Detector Array for the search of neutrinoless $\beta\beta$ decay of ^{76}Ge at LNGS, Proposal, http://www.mpi-hd.mpg.de/GERDA

[2] H.V. Klapdor-Kleingrothaus *et al.*, Search for neutrinoless double beta decay with enriched 76Ge in Gran Sasso 1990-2003, Phys. Lett. B 586 (2004) 198

16

[3] G. Douysset *et al.*, Determination of the ^{76}Ge double beta Q value, Phys. Rev. Lett. 86 (2001) 4259

[4] G. Heusser, Low-radioactivity background techniques, Ann. Rev. Nucl. Part. Scie. 45 (1995) 543

[5] H.V. Klapdor-Kleingrothaus *et al.*, Data acquisition and analysis of the ^{76}Ge double beta experiment in Gran Sasso 1990-2003, Nucl. Instr. Meth. A 522 (2004) 371

[6] D.-M. Mei and A. Hime, Muon-induced background study for underground laboratories, Phys. Rev. D 73 (2006) 053004

[7] Majorana Collaboration, White paper on the Majorana zero-neutrino double-beta decay experiment, nucl-ex/0311013 (2003)

[8] MACRO Collaboration, M. Ambrosio *et al.*, Vertical muon intensity measured with MACRO at the Gran Sasso Laboratory, Phys. Rev. D 52 (1995) 3793

[9] MACRO Collaboration, M. Ambrosio *et al.*, Measurement of the residual energy of muons in the Gran Sasso underground laboratories, Astrop. Phys. 19 (2003) 313

[10] P. Lipari and T. Stanev, Propagation of multi-TeV muons, Phys. Rev. D 44 (1991) 3543

[11] MACRO Collaboration, S. Ahlen *et al.*, Muon astronomy with the MACRO detector, Ap. J. 412 (1993) 412

[12] Borexino Collaboration, G. Alimonti *et al.*, Science and technology of Borexino: a real-time detector for low energy solar neutrinos, Astrop. Phys. 16 (2002) 205

[13] GEANT4 Collaboration, S. Agostinelli *et al.*, GEANT4: A Simulation Toolkit, Nucl. Instr. Meth. A 506 (2003) 250; GEANT4 Collaboration, J. Allison *et al.*, GEANT4 developments and applications, IEEE Trans. Nucl. Scie. 53 (2006) 270

[14] M. Bauer *et al.*, MAGE: a Monte Carlo framework for the Gerda and Majorana double beta decay experiments, Journal of Physics, Conf. Series 39 (2006) 362; S. Belogurov *et al.*, MAGE, a simulation framework for 76-Ge based neutrinoless double beta decay experiments, to appear in Journal of Physics, Conf. Series

[15] GEANT4 website, http://geant4.cern.ch

[16] C. Dörr and H.V. Klapdor-Kleingrothaus, New Monte-Carlo simulation of the Heidelberg-Moscow double beta decay experiment, Nucl. Instr. Meth. A 513 (2003) 596

[17] M. Bauer *et al.*, Simulations of muon-induced neutron background with Geant4, Proceedings of the V International Workshop on the Identification of Dark Matter, Edinburgh UK 6-10 September 2004, World Scientific 2005, 494

17

[18] J. Ljungvall and J. Nyberg, A study of fast neutron interactions in high-purity germanium detectors, Nucl. Instr. Meth. A 546 (2005) 553

[19] G.A.P. Cirrone *et al.*, Precision validation of Geant4 electromagnetic physics, IEEE Nucl. Sci. Symp., Conf. Record 2003 , IEEE 1 (2003) 482; K. Amako *et al.*, Validation of Geant4 electromagnetic physics versus the NIST databases, IEEE Trans. Nucl. Scie. 52 (2005) 910

[20] E. Poon and F. Verhaegen, Accuracy of the photon and electron physics in Geant4 for radiotherapy applications, Med. Phys. 32 (2005) 1696

[21] M. Cribier *et al.*, The muon induced background in the Gallex experiment, Astrop. Phys. 6 (1997) 129

[22] H.M. Araujo *et al.*, Muon-induced neutron production and detection with GEANT4 and FLUKA, Nucl. Instrum. Meth. A 545 (2005) 398

[23] LVD Collaboration, M. Aglietta *et al.*, Measurement of the neutron flux produced by cosmic ray muons with LVD at Gran Sasso, Proc. of 26th Intern. Cosmic Ray Conf., Salt Lake City (USA), August 17-25, 1999, hep-ex/9905047 v1 (1999)

[24] A. Fassò *et al.*, FLUKA: a multi-particle transport code, CERN-2005-10 (2005), INFN/TC-05/11, SLAC-R-773

[25] S. Eidelman *et al.*, Review of Particle Physics, Sect. 27, Phys. Lett. B 592 (2004) 1

[26] H. Wulandari *et al.*, Neutron background studies for the CRESST dark matter experiment, hep-ex/0401032 v1 (2004)

[27] L. Baudis *et al.*, High purity germanium detector ionization pulse shapes of nuclear recoils, gamma interactions and microphonism, Nucl. Instrum. Meth. A 418 (1998) 348

[28] I. Abt *et al.*, Background suppression in neutrinoless double beta decay experiments using segmented detectors - a Monte Carlo study, submitted to Nucl. Instr. Meth. A

[29] D. Gonzalez *et al.*, Pulse shape discrimination in the IGEX experiment, Nucl. Instr. Meth. A 515 (2003) 634

[30] J. Hellmig and H.V. Klapdor-Kleingrothaus, Identification of single-site events in germanium detectors by digital pulse shape analysis, Nucl. Instr. Meth. A 455 (2000) 638; B. Majorovits and H.V. Klapdor-Kleingrothaus, Digital pulse shape analysis by neural networks for the Heidelberg-Moscow double-beta-decay experiment, Eur. Phys. J. A 6 (1999) 463

[31] L. Oberauer and S. Schönert, Status report on the Borexino muon identification system, Borexino Internal Note (1997); C. Lendvai, Identification of muon-induced signals in the deep underground neutrino-scintillator-detector Borexino, Ph. D. thesis, Technische Universität München (2005)

[32] LBNL Isotopes Project Nuclear Data Dissemination Home Page (available at http://ie.lbl.gov/toi.html)

[33] W.S. Lyon and J.S. Eldridge, Radioactive Ge^{77} and Ge^{77m}, Phys. Rev. 107 (1957) 1056

[34] A.R. Farhan and B. Singh, Nuclear Data Sheets for A=77, Nucl. Data Sheets 81 (1997) 417